

Remnant evolution after a carbon-oxygen white dwarf merger

S.-C. Yoon^{1,2*}, Ph. Podsiadlowski³ and S. Rosswog⁴

¹*Astronomical Institute "Anton Pannekoek", University of Amsterdam, Kruislaan 403, 1098 SJ, Amsterdam, The Netherlands*

²*Department of Astronomy & Astrophysics, University of California, Santa Cruz, CA95064, USA*

³*Department of Astrophysics, University of Oxford, Keble Road, Oxford OX1 3RH, UK*

⁴*School of Engineering and Science, Jacobs University Bremen†, Campus Ring1, Bremen 28759, Germany*

Accepted/ Received

ABSTRACT

We systematically explore the evolution of the merger of two carbon-oxygen (CO) white dwarfs. The dynamical evolution of a $0.9 M_{\odot} + 0.6 M_{\odot}$ CO white dwarf merger is followed by a three-dimensional SPH simulation. The calculation uses a state-of-the-art equation of state that is coupled to an efficient nuclear reaction network that accurately approximates all stages from helium burning up to nuclear statistical equilibrium. We use an elaborate prescription in which artificial viscosity is essentially absent, unless a shock is detected, and a much larger number of SPH particles than earlier calculations. Based on this simulation, we suggest that the central region of the merger remnant can, once it has reached quasi-static equilibrium, be approximated as a differentially rotating CO star, which consists of a slowly rotating cold core and a rapidly rotating hot envelope surrounded by a centrifugally supported disc. We construct a model of the CO remnant that mimics the results of the SPH simulation using a one-dimensional hydrodynamic stellar evolution code and then follow its secular evolution, where we include the effects of rotation on the stellar structure and the transport of angular momentum. The influence of the Keplerian disc is implicitly treated by considering mass accretion from the disc onto the hot envelope. The stellar evolution models indicate that the growth of the cold core is controlled by neutrino cooling at the interface between the core and the hot envelope, and that carbon ignition in the envelope can be avoided despite high effective accretion rates. This result suggests that the assumption of forced accretion of cold matter that was adopted in previous studies of the evolution of double CO white dwarf merger remnants may not be appropriate. Specifically we find that off-center carbon ignition, which would eventually lead to the collapse of the remnant to a neutron star, can be avoided if the following conditions are satisfied: (1) when the merger remnant reaches quasi-static equilibrium, the local maximum temperature at the interface between the core and the envelope must be lower than the critical limit for carbon-ignition. (2) Angular-momentum loss from the central merger remnant should not occur on a time scale shorter than the local neutrino cooling time scale at the interface. (3) The mass-accretion rate from the centrifugally supported disc must be sufficiently low ($\dot{M} \lesssim 5 \times 10^{-6} \dots 10^{-5} M_{\odot} \text{ yr}^{-1}$). Our results imply that at least some products of double CO white dwarfs merger may be considered good candidates for the progenitors of Type Ia supernovae. In this case, the characteristic time delay between the initial dynamical merger and the eventual explosion would be $\sim 10^5$ yr.

Key words: Stars: evolution – Stars: white dwarf – Stars: accretion – Supernovae: general –

1 INTRODUCTION

The coalescence of two carbon-oxygen (CO) white dwarfs with a combined mass in excess of the Chandrasekhar limit has long been considered a promising path towards a Type Ia supernova (SN Ia; Iben & Tutukov 1984; Webbink 1984). Indeed, in the last few

years, a few massive double CO white dwarf systems have been found that have periods short enough for them to merge within a Hubble time (e.g. Napiwotzki et al. 2002, 2004). This double-degenerate (DD) scenario can also easily explain the lack of hydrogen and helium lines in most SN Ia spectra and the occurrence of SNe Ia both in old and young star-forming systems (e.g. Branch et al. 1995).

Theoretically, the final fate of double CO white dwarf mergers has been much debated. Previous studies assumed that the dynamical disruption of the Roche-lobe filling secondary should lead

* E-mail: scyoon@science.uva.nl (SCY); podsi@astro.ox.ac.uk (PhP); s.rosswog@iu-bremen.de (SR)

† formerly International University Bremen

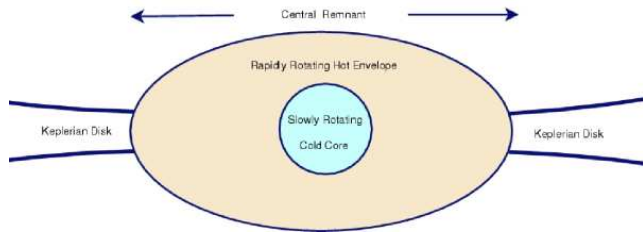


Figure 1. Schematic illustration of the configuration of the remnant of a double CO white dwarf merger once quasi-static equilibrium has been established.

to the formation of a thick disc around the primary white dwarf (Tutukov & Yungelson 1979; Mochkovitch & Livio 1989, 1990). Therefore, accretion of CO-rich matter from the thick disc onto the central cold white dwarf has been studied for investigating the evolution of such mergers by many authors (Nomoto & Iben 1985; Saio & Nomoto 1985, 1998, 2004; Piersanti et al. 2003a,b). As accretion rates from the thick disc should be close to the Eddington limit ($\dot{M} \approx 10^{-5} M_{\odot} \text{yr}^{-1}$), most of those studies concluded that carbon ignition in the envelope of the accreting white dwarf is an inevitable consequence of such rapid accretion of CO-rich matter. Once carbon ignites off-center, the burning flame propagates inwards on a relatively short time scale (~ 5000 yr), and the CO white dwarf is transformed into an ONeMg white dwarf (Saio & Nomoto 1985, 1998). When the mass of the ONeMg white dwarf approaches the Chandrasekhar limit, electron capture onto Ne and Mg is expected to lead to the gravitational collapse of the white dwarf to a neutron star (Nomoto & Kondo 1991; see Dessart et al. (2006) for a recent study of such collapse).

However, the evolution of the remnants of double CO white dwarf mergers is not yet well understood. For instance, it has been debated whether the accretion rate decreases when the accreting white dwarf reaches critical rotation (Piersanti et al. 2003a; Saio & Nomoto 2004). More importantly, the canonical description of the merger remnant as a primary white dwarf + thick disc system is clearly an oversimplification. In previous three-dimensional smoothed particle hydrodynamics (SPH) simulations (Benz et al. 1990; Segretain, Chabrier & Mochkovitch 1997; Guerrero et al. 2004; see also Sect. 2), a large fraction of the disrupted secondary and the outermost layers of the primary form an extended hot envelope around the cold core containing most of the primary mass. The rest of the secondary mass becomes a centrifugally supported disc in the outermost layers of the merger remnant. Interestingly, the merger remnant reaches a state of quasi-static equilibrium within a few minutes from the onset of the dynamical disruption of the secondary. As the structure of the cold core plus the hot envelope appears to have a fairly spheroidal shape (see below) rather than the toroidal shape obtained with a zero-temperature equation of state (Mochkovitch & Livio 1989, 1990), the merger remnant may be better described as a *differentially rotating single CO star* consisting of a slowly rotating cold core and a rapidly rotating hot extended envelope surrounded by a Keplerian disc, as illustrated in Fig. 1, than the previously adopted primary white dwarf + thick disc system. The further evolution of the merger must therefore be determined by the thermal cooling of the hot envelope and the redistribution of the angular momentum inside the central remnant, and accretion of matter onto the envelope from the Keplerian disc.

With this new approach to the problem in mind, we here revisit both the dynamical and the secular evolution of double CO

white dwarf mergers. In the following section (Sect. 2), we present the numerical results of an SPH simulation of the dynamical evolution of the coalescence of a $0.9 M_{\odot}$ WD and a $0.6 M_{\odot}$ CO white dwarf up to the stage of quasi-hydrostatic equilibrium, and we carefully investigate the structure of the merger remnant. In Sect. 3, we construct models of the central remnant in quasi-static equilibrium state (primary + hot extended envelope) which mimic the SPH result and calculate the thermal evolution of the merger remnant using a hydrodynamic stellar evolution code. In particular, the conditions for avoiding off-center carbon ignition are systematically explored. In Sect. 4, we conclude this work by discussing uncertainties in our assumptions, the implications for Type Ia supernovae and future work.

2 DYNAMICAL EVOLUTION OF THE MERGER

Before discussing the subsequent thermal evolution after the coalescence of a double CO white dwarf coalescence binary, we investigate the configuration of the remnant in quasi-static equilibrium in some detail. For this purpose, we have carried out a SPH simulation of the dynamical process of the coalescence of two CO white dwarfs of $0.9 M_{\odot}$ and $0.6 M_{\odot}$, respectively. Our simulation uses a 3D smoothed particle hydrodynamics (SPH) code that is an offspring of a code developed to simulate neutron star mergers (Rosswog et al. 2000; Rosswog & Davies 2002; Rosswog & Liebendörfer 2003). It uses an artificial viscosity scheme with time-dependent parameters (Morris & Monaghan 1997). In the absence of shocks, the viscosity parameters have a very low value ($\alpha = 0.05$ and $\beta = 0.1$; most SPH implementations use values of $\alpha = 1...1.5$ and $\beta = 2...3$); if a shock is detected, a source term (Rosswog et al. 2000) guarantees that the parameters rise to values that are able to resolve the shock properly without spurious post-shock oscillations. To suppress artificial viscosity forces in pure shear flows, we additionally apply a switch originally suggested by Balsara (1995).

To account for the energetic feedback onto the fluid from nuclear transmutations, we use a minimal nuclear reaction network developed by Hix et al. (1998). It couples a conventional α -network stretching from He to Si with a quasi-equilibrium-reduced α -network. Although a set of only seven nuclear species is used, this network reproduces the energy generation of all burning stages from He-burning to NSE very accurately. For details and tests we refer to Hix et al. (1998). We use the HELMHOLTZ equation of state (EOS), developed by the Center for Astrophysical Thermonuclear Flashes at the University of Chicago. This EOS allows to freely specify the chemical composition of the gas and can be coupled to nuclear reaction networks. The electron/positron equation of state has been calculated without approximations, i.e. it makes no assumptions about the degree of degeneracy or relativity; the exact expressions are integrated numerically to machine precision. The nuclei in the gas are treated as a Maxwell-Boltzmann gas, the photons as blackbody radiation. The EOS is used in tabular form with densities ranging from $10^{-10} \leq \rho Y_e \leq 10^{11} \text{ g cm}^{-3}$ and temperatures from 10^4 to 10^{11} K. A sophisticated, biquintic Hermite polynomial interpolation is used to enforce thermodynamic consistency (i.e. the Maxwell-relations) at interpolated values (Timmes & Swesty 2000).

We use a MacCormack predictor-corrector method (e.g. Lomax et al. 2001) with individual particle time steps to evolve the fluid. With our standard parameters for the tree-opening criterion and the integration, this time marching implementation con-

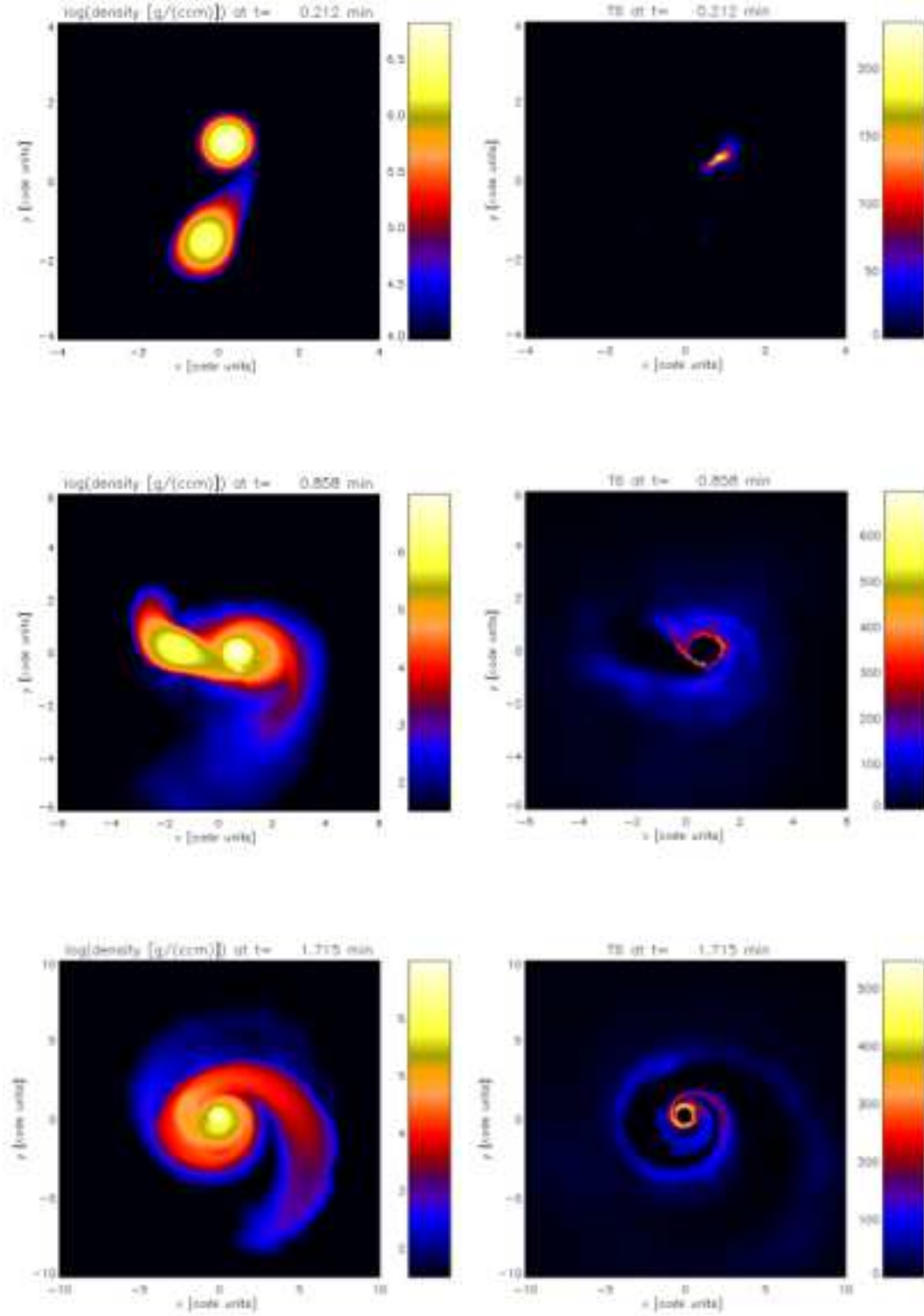


Figure 2. Dynamical evolution of the coalescence of a $0.6 M_{\odot} + 0.9 M_{\odot}$ CO white dwarf binary. The panels in the left column show the density in the orbital plane, the panels in the right column the temperature in units of 10^6 K. Lengths are in code units ($= 10^9$ cm).

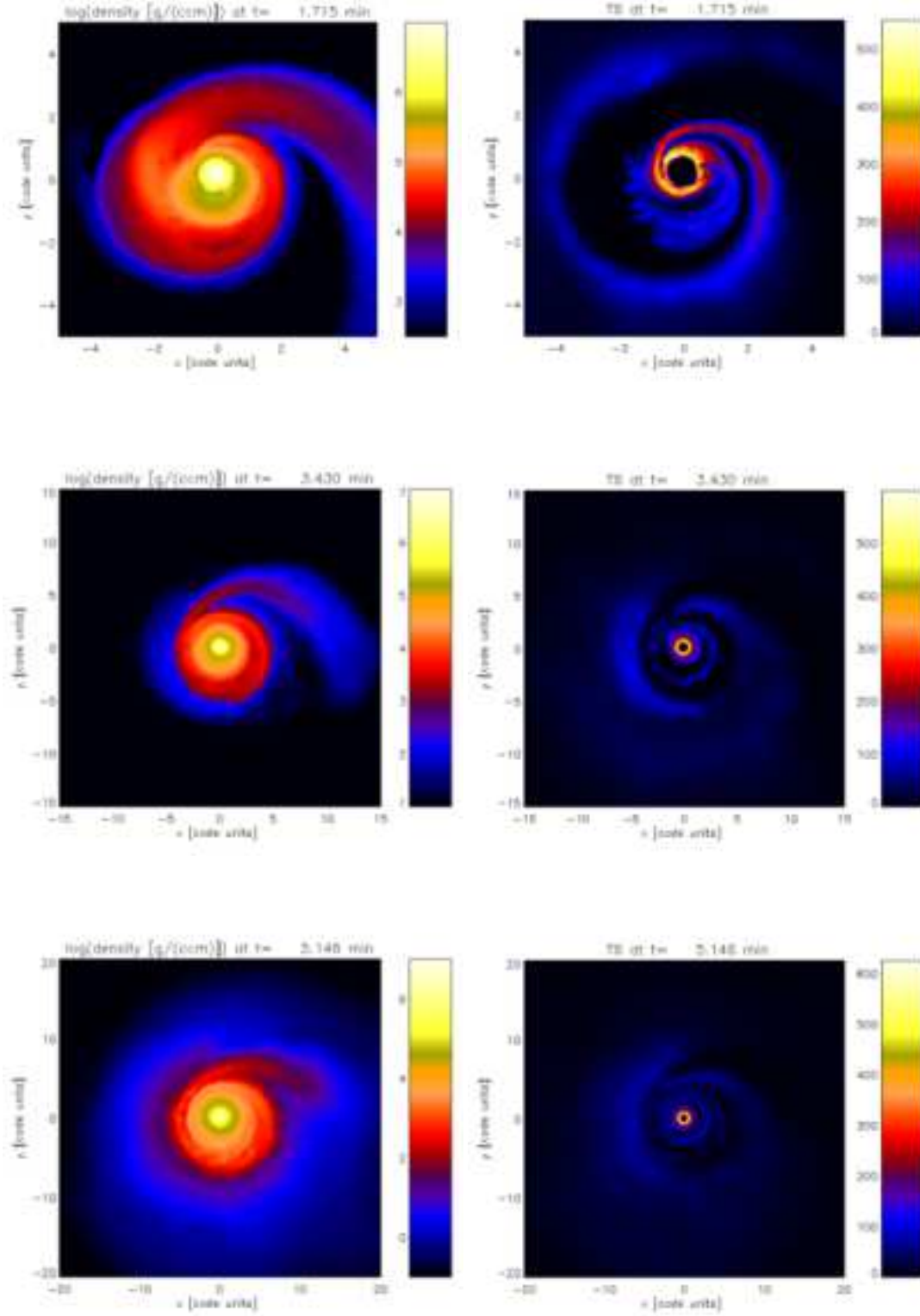


Figure 3. Dynamical evolution of the coalescence of a $0.6 M_{\odot} + 0.9 M_{\odot}$ CO white dwarf binary. Continued from Fig. 2.

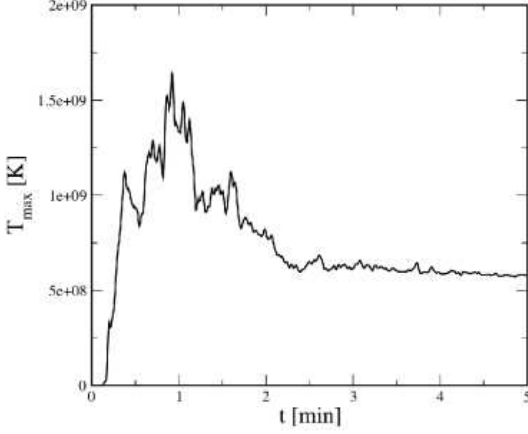


Figure 4. The evolution of the local peak of temperature during the merger of two CO white dwarfs of $0.6 M_{\odot}$ and $0.9 M_{\odot}$, respectively, as a function of time after the onset of the simulation.

serves the total energy to better than 4×10^{-3} and the total angular momentum to better than 2×10^{-4} . Note that this could, in principle, be improved even further by taking into account the so-called “grad-h”-terms (Springel & Hernquist 2002; Monaghan 2002; Price 2004) and extra-terms arising from adapting gravitational smoothing terms (Price & Monaghan 2006).

To avoid numerical artifacts, we only use equal mass SPH particles. For the initial conditions, we therefore stretch a uniform particle distribution according to a function that has been derived from solving the 1D stellar structure equations. This technique is described in detail in Rosswog, Ramirez-Ruiz & Hix (2007). This particle setup is then further relaxed with an additional damping force (e.g. Rosswog, Speith & Wynn 2004) so that the particles can settle into their true equilibrium configuration. The calculations are performed with 2×10^5 SPH particles, a much larger particle number than could be afforded by previous calculations, and run up to a much longer evolutionary time (5 minutes) than previous calculations (see Table 1).

Figs. 2 and 3 show the dynamical evolution of the merging process of the double white dwarf system considered in this study. The panel in the left columns show the densities and the panel in the right columns the temperatures (in units of 10^6 K) in the orbital plane. The secondary is completely disrupted within 1.7 minutes, and mass accretion onto the primary induces local heating near the surface of the primary. Fig. 4 shows the evolution of the maximum temperature as a function of time. The peak in temperature reaches 1.7×10^9 K at $t \simeq 1.0$ min, where $t = 0.0$ marks the moment when the simulation starts. Carbon ignites when $T \gtrsim 10^9$ K, but nuclear burning is quenched soon due to the local expansion of the hottest region, as is also observed in the simulations of Guerrero et al. (2004). The total amount of energy released due to nuclear burning is about 10^{45} erg.

Segretain, Chabrier & Mochkovitch (1997) considered the same initial white dwarf masses as in the present study. But they adopted the original artificial viscosity prescription of Monaghan & Varnas (1988), which is known to introduce spurious forces in shear flows, and they did not include nuclear burning (Table 1). By the end of their calculation ($t = 1.56$ min), T_{\max} reached 8×10^8 K, while in our simulation, it decreases to 8×10^8 K only when $t \sim 1.7$ min. Interestingly, T_{\max} decreases further afterwards in our calculation, as shown in Fig. 4, and reaches a steady

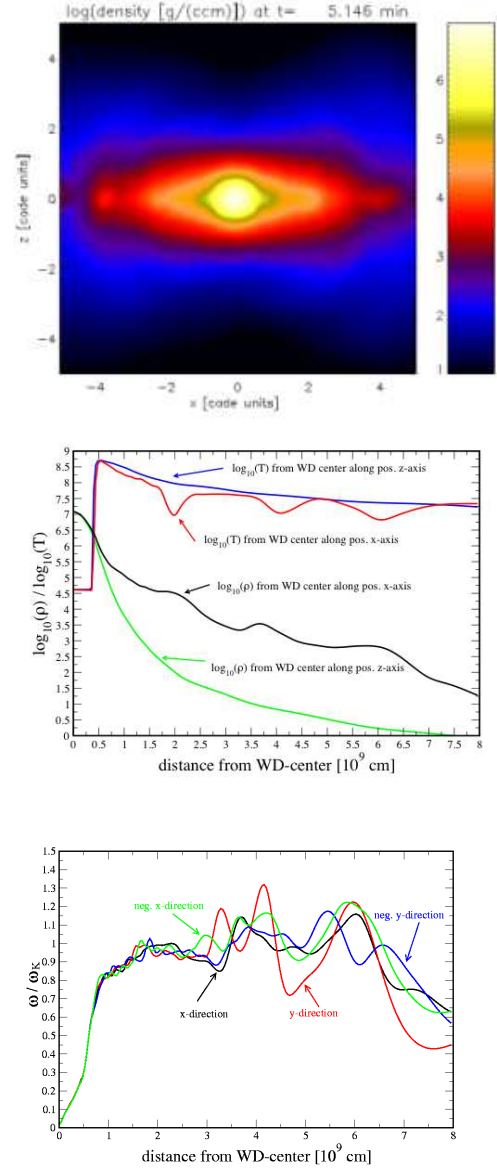


Figure 5. *Top:* Density contour of the merger remnant in the $x - z$ plane at $t = 5.3$ min. Here one code unit corresponds to 10^9 cm. *Middle:* Thermodynamic structure of the merger remnant at $t = 5.31$ min: shown are the temperature and the density as a function of distance from the centre, along the positive x - and z -axis, as indicated. *Bottom:* Angular velocity in units of the local Keplerian value at $t = 5.31$ min, along the positive/negative x - and y -axis of the merger remnant.

value at $T_{\max} \simeq 5.6 \times 10^8$ K when $t \gtrsim 2.5$ min. In the other calculations by Benz et al. (1990) and Guerrero et al. (2004), the dynamical evolution of the merger was not followed for more than 2 minutes either, and we cannot directly compare our results to theirs. However, we suspect that T_{\max} would also decrease further in the systems they considered if they had continued their calculations for a longer evolutionary time. It should also be noted that energy dissipation by artificial viscosity might lead to overheating, and that thermal diffusion – which may play an important role in the outer-

most layers – is not considered in the present study. It is thus likely that T_{\max} in the quasi-static equilibrium state may be even lower in reality than in our simulation.

Fig. 5 shows the structure of the merger remnant at quasi-static equilibrium. The central region with $R \lesssim 10^9$ cm ($M_r \lesssim 1.1 M_\odot$) has a fairly spheroidal shape, and a centrifugally supported disc appears at $R \gtrsim 10^9$ cm where the angular velocity is close to the Keplerian value. The fraction of the secondary mass contained in the Keplerian disc is larger in our simulation (about 67%) than in Segretain, Chabrier & Mochkovitch (1997) (about 41 %). The innermost core ($R \lesssim 3 \times 10^8$ cm; $M_r \lesssim 0.6 M_\odot$) is essentially isothermal, and the temperature has its peak value ($T \simeq 5.6 \times 10^8$ K) at $R \simeq 5 \times 10^8$ cm and $M_r \simeq 0.85 M_\odot$. The disc material extends over 4×10^9 cm along the z -axis as the temperature is still high; if thermal diffusion were included, the disc would become much thinner on a short time scale of a few hours. Therefore, our simulation confirms the remnant structure at quasi-static equilibrium that is illustrated in Fig. 1. In the next section, we investigate the secular evolution of the merger from such a quasi-static equilibrium state.

3 SECULAR EVOLUTION OF THE MERGER REMNANT

3.1 Physical assumptions and methods

Our SPH simulation shows that the remnant of the merger of two CO white dwarfs ($0.9 M_\odot + 0.6 M_\odot$) in the state of quasi-static equilibrium has the following features (see Fig. 6):

- (i) The core is cold and nearly isothermal.
- (ii) The local peak of temperature (T_p) is located at a mass coordinate slightly less than the primary mass.
- (iii) A steep gradient in temperature appears at the interface between the core and the local peak of temperature.
- (iv) The interface is rather widely extended into the primary ($\Delta M_{\text{interface}} \approx 33$ % of the primary mass), and the mass of the quasi-isothermal cold core (M_{core}) is about 77 % of the primary mass.
- (v) The mass of the outer envelope above the local peak of temperature contains about 33 % of the mass of the secondary, and the rest of the secondary forms a Keplerian disc.

Let us define T_p as the local peak of temperature at quasi-static equilibrium, M_{CM} as the mass of the central remnant (cold core + hot envelope), and M_p as the location of T_p in the mass coordinate (i.e., $M_p = M_{\text{core}} + \Delta M_{\text{interface}}$; see Fig. 6). To construct models of the central remnant, we use a one-dimensional hydrodynamic stellar evolution code which incorporates the effects of rotation on the stellar structure, transport of angular momentum due to the shear instability, Eddington-Sweet circulation, and the Goldreich, Schubert and Fricke instability, and dissipation of rotational energy due to shear motions. The effects of magnetic fields are neglected (see Sec. 4). More details about the code are described in (Yoon & Langer 2004; hereafter YL04) and references therein.

In order to mimic the temperature profile of the central remnant as obtained from the SPH simulation, we artificially deposit energy in the envelope, using the following prescription for a white dwarf with $M = M_{\text{CR}}$:

$$e(M_r) = A(T'(M_r) - T(M_r)) \text{ [erg g}^{-1} \text{ s}^{-1}], \quad (1)$$

where

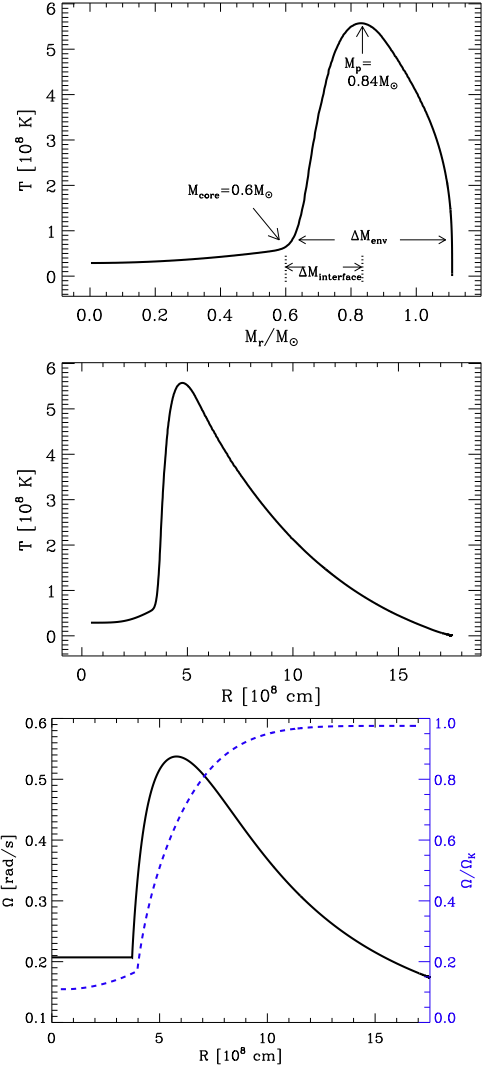


Figure 6. Initial model of the central remnant for sequences Sa1 – Sa11. The top and middle panels show temperature as a function of the mass coordinate and radius, respectively. The solid curve in the bottom panel gives the angular-velocity profile as a function of radius. The dashed curve denotes the angular velocity in units of the local Keplerian value.

$$T'(M_r) = \begin{cases} 3 \cdot 10^7 \text{ K} + (7 \cdot 10^7 \text{ K} - 3 \cdot 10^7 \text{ K}) \left(\frac{M_r}{M_{\text{core}}} \right)^2, & \text{if } M_r < M_{\text{core}}, \\ T_p - (T_p - 7 \cdot 10^7 \text{ K}) \left(\frac{M_p - M_r}{M_p - M_{\text{core}}} \right)^2, & \text{if } M_{\text{core}} \leq M_r \leq M_p, \\ C - (C - T_p) \left(\frac{\log[\rho(M_r)/\rho_s]}{\log[\rho(M_p)/\rho_s]} \right)^2, & \text{if } M_r > M_p. \end{cases} \quad (2)$$

In this way, the temperature profile in the central remnant model follows $T'(M_r)$. Here, A and C are constants. We use $A = 10^5 \text{ erg g}^{-1} \text{ s}^{-1} \text{ K}^{-1}$ and $C = 2 \times 10^8 \text{ K}$ in most cases.

A rotational profile is imposed as

Table 1. Comparison of SPH simulations of double CO white dwarf mergers. The columns list: M_1 and M_2 : the masses of the primary and the secondary, respectively; NoP: the total number of particles used; ν_{sph} : the type of artificial viscosity employed, ‘std.’ refers to Monaghan & Varnas (1988); Network: type of nuclear network employed; t_{sim} : evolutionary time that has elapsed by the end of the calculation; T_{max} : maximum temperature obtained during the simulation; and T_{p} : the local peak of temperature at the end of the calculation

Ref.*	M_1	M_2	NoP	ν_{sph}	Network	t_{sim}	T_{max}	T_{p}
1	1.2 M_{\odot}	0.9 M_{\odot}	$\sim 7 \times 10^3$	std.	None	51 sec.	?	$\sim 10^9$ K
2	0.8 M_{\odot}	0.6 M_{\odot}	$\sim 4 \times 10^4$	std. + Balsara-switch	alpha network	50 sec.	1.4×10^9 K	?
2	1.0 M_{\odot}	0.6 M_{\odot}	$\sim 4 \times 10^4$	std. + Balsara-switch	alpha network	65 sec.	1.6×10^9 K	?
2	1.0 M_{\odot}	0.8 M_{\odot}	$\sim 4 \times 10^4$	std. + Balsara-switch	alpha network	65 sec.	2.0×10^9 K	?
3	0.9 M_{\odot}	0.6 M_{\odot}	$\sim 6 \times 10^4$	std	None	1.56 min.	?	$\sim 7 \times 10^8$ K
4	0.9 M_{\odot}	0.6 M_{\odot}	2×10^5	see Rosswog et al. (2000)	QSE-alpha network	5.3 min.	1.7×10^9 K	5.6×10^8 K

*1: Benz et al. (1990), 2: Guerrero et al. (2004), 3: Segretain, Chabrier & Mochkovitch (1997); 4: Present Study

Table 2. Merger remnant model sequences. Each column lists the following: No.: sequence label, M_{CR} : mass of the central remnant, M_{core} : mass of the quasi-isothermal core, M_{p} : location of the local peak of temperature in the mass coordinate, T_{p} : the local peak of temperature, ρ_{p} : density at $M_{\text{r}} = M_{\text{p}}$, τ_{J} : adopted time scale for angular momentum loss according to Eq. (4), \dot{M}_{acc} : adopted mass accretion rate from the Keplerian disc, C-ig: off-center ignition of carbon, $M_{\text{WD,ig}}$: total mass of the central remnant when off-center carbon ignition occurs, $M_{\text{r,ig}}$: location of off-center carbon ignition in the mass coordinate.

No.	M_{CR} [M_{\odot}]	M_{core} [M_{\odot}]	M_{p} [M_{\odot}]	T_{p} [10^8 K]	ρ_{p} [10^6 g/cm 3]	τ_{J} [yr]	\dot{M}_{acc} $10^{-6} M_{\odot}$ /yr	C-ig	$M_{\text{WD,ig}}$ [M_{\odot}]	$M_{\text{r,ig}}$ [M_{\odot}]
Sa1	1.11	0.6	0.84	5.6	0.8	∞	0.0	No	-	-
Sa2	1.11	0.6	0.84	5.6	0.8	10^2	0.0	Yes	1.11	0.80
Sa3	1.11	0.6	0.84	5.6	0.8	10^3	0.0	Yes	1.11	0.80
Sa4	1.11	0.6	0.84	5.6	0.8	10^4	0.0	Yes	1.11	0.85
Sa5	1.11	0.6	0.84	5.6	0.8	10^5	0.0	No	-	-
Sa6	1.11	0.6	0.84	5.6	0.8	10^5	10.0	Yes	1.34	1.09
Sa7	1.11	0.6	0.84	5.6	0.8	10^5	5.0	Yes	1.34	1.20
Sa8	1.11	0.6	0.84	5.6	0.8	10^5	2.0	No	-	-
Sa9	1.11	0.6	0.84	5.6	0.8	10^5	1.0	No	-	-
Sa10	1.11	0.6	0.84	5.6	0.8	$5 \cdot 10^5$	5.0	No	-	-
Sa11	1.11	0.6	0.84	5.6	0.8	$5 \cdot 10^5$	1.0	No	-	-
Aa1	1.25	0.6	0.93	5.0	2.3	∞	0.0	No	-	-
Aa2	1.25	0.6	0.93	5.0	2.3	10^2	0.0	Yes	1.250	0.90
Aa3	1.25	0.6	0.93	5.0	2.3	10^3	0.0	Yes	1.250	0.92
Aa4	1.25	0.6	0.93	5.0	2.3	10^4	0.0	Yes	1.250	1.12
Aa5	1.25	0.6	0.92	5.0	2.3	10^5	0.0	No	-	-
Aa6	1.25	0.6	0.92	5.0	2.3	10^6	0.0	No	-	-
Aa7	1.25	0.6	0.92	5.0	2.3	10^5	10.0	Yes	1.360	1.20
Aa8	1.25	0.6	0.92	5.0	2.3	10^5	5.0	No	-	-
Aa9	1.25	0.6	0.92	5.0	2.3	10^5	1.0	No	-	-
Aa10	1.25	0.6	0.92	5.0	2.3	10^6	10.0	Yes	1.382	1.22
Ab1	1.25	0.7	0.92	5.0	3.1	∞	0.0	No	-	-
Ab2	1.25	0.7	0.92	5.0	3.1	10^3	0.0	Yes	1.250	0.97
Ab3	1.25	0.7	0.92	5.0	3.1	10^4	0.0	No	-	-
Ab4	1.25	0.7	0.92	5.0	3.1	10^5	0.0	No	-	-
Ab5	1.25	0.7	0.92	5.0	3.1	10^5	10.0	Yes	1.344	1.21
Ab6	1.25	0.7	0.92	5.0	3.1	10^5	5.0	No	-	-
Ac1	1.25	0.5	0.88	5.9	1.6	∞	0.0	Yes	1.250	0.84
Ad1	1.25	0.6	0.92	6.0	1.8	∞	0.0	Yes	1.250	0.90
Ad2	1.25	0.6	0.92	6.0	1.8	10^6	5.0	Yes	1.252	0.90
Ae1	1.25	0.6	0.90	6.8	1.5	∞	0.0	Yes	1.250	0.87
Ba1	1.363	0.82	0.95	5.0	12.2	∞	0.0	No	-	-
Ba2	1.363	0.82	0.95	5.0	12.2	10^2	0.0	Yes	1.363	0.95
Ba3	1.363	0.82	0.95	5.0	12.2	10^3	0.0	Yes	1.363	1.12
Ba4	1.363	0.82	0.95	5.0	12.2	10^4	0.0	No	-	-
Ba5	1.363	0.82	0.95	5.0	12.2	10^5	0.0	No	-	-
Ba6	1.363	0.82	0.95	5.0	12.2	10^5	10.0	Yes	1.398	1.34
Ba7	1.363	0.82	0.95	5.0	12.2	10^5	5.0	Yes	1.483	1.43
Ba8	1.363	0.82	0.95	5.0	12.2	10^5	1.0	No	-	-
Ta1	1.25	0.60	0.86	5.0	28.8	∞	0.0	No	-	-

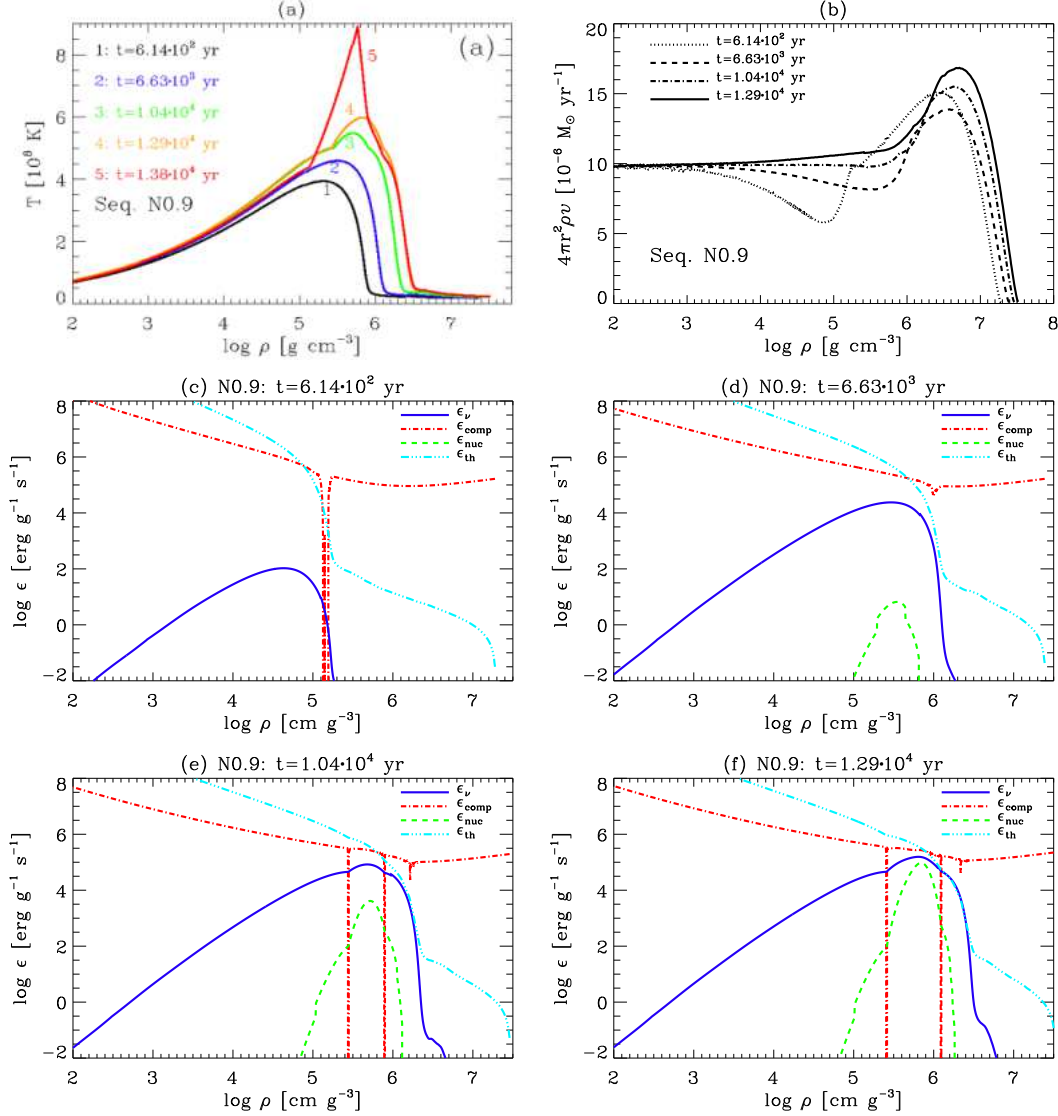


Figure 7. (a) Evolution of a non-rotating white dwarf accreting with a constant accretion rate of $\dot{M} = 10^{-5} M_{\odot} \text{ yr}^{-1}$ with an initial mass of $0.9 M_{\odot}$ (Seq. N0.9) in the density – temperature plane. (b) The local effective accretion rate ($\dot{M}_{\text{eff},r} := 4\pi r^2 \rho v$) as a function of density in Seq. N0.9, at different evolutionary epochs as indicated by the labels. (c) – (f) The rates of energy loss/production due to neutrino (ϵ_ν) cooling, compressional heating (ϵ_{comp}), nuclear energy generation (ϵ_{nuc}) and thermal diffusion (ϵ_{th}) at different evolutionary epochs. Note that here ϵ_ν , ϵ_{comp} and ϵ_{nuc} represent the values which are used in the evolutionary calculations, while ϵ_{th} is an order-of-magnitude estimate according to Eq. (7).

$$\Omega(M_r) = \begin{cases} \Omega_O, & \text{if } M_r < M_{\text{core}}, \\ \left[\omega_O + (1 - \omega_O) \left(\frac{M_r - M_{\text{core}}}{M_{\text{CR}} - M_{\text{core}}} \right)^{0.9} \right] \sqrt{\frac{GM_r}{r^3}}, & \text{if } M_r \geq M_{\text{core}}, \end{cases} \quad (3)$$

where $\Omega_O = 0.2 \sqrt{GM_{\text{CR}}/R^3}$ and $\omega_O = \Omega_O / \sqrt{GM_{\text{core}}/r_{\text{core}}^3}$. As shown in Fig. 6, this simple assumption gives a rotational velocity profile that is morphologically similar to that found in the SPH simulation: a steep gradient at the interface between the core and the envelope, and a local peak in the envelope. Within our 1-D approximation of the effects of rotation, the exact shape of the rotational velocity profile does not affect the main conclusions of the present work for the following reasons. Firstly, the velocity gradient at the interface is adjusted to the threshold value for the dynamical shear instability on a very short time scale (see below, and discus-

sions in YL04). Secondly, our 1-D approximation underestimates the effect of the centrifugal force on the stellar structure in layers which rotate more rapidly than about 60 % critical (YL04), and uncertainties due to this limit are much greater than due to the shape of $\Omega(r)$ in the outer layers of the envelope. Possible uncertainties due to this limitation are critically discussed in Sect. 4.

The central remnant may lose angular momentum by outward angular momentum transport into the Keplerian disc (Popham & Narayan 1991; Paczyński 1991) and/or by the gravitational wave radiation, e.g., due to the r -mode instability (Andersson 1998; Friedman & Morsink 1998). Our code cannot properly describe any of these effects, and here we consider them simply by assuming a constant time scale for the angular momentum loss (τ_J ; see Knaap 2004; cf. Piersanti et al. 2003a), such that the specific

Table 3. Accreting white dwarf model sequences with a constant accretion rate ($\dot{M} = 10^{-5} M_{\odot}/\text{yr}$). The columns list: No: sequence label, M_{init} : initial mass, $\log L_{\text{init}}/L_{\odot}$: initial luminosity, $M_{\text{WD,ig}}$: the total mass of the white dwarf when carbon ignites off-center, and $M_{\text{r,ig}}$: location of carbon ignition in the mass coordinate. Sequences with ‘N’ are for non-rotating models, and ‘R’ for rotating models.

No	M_{init}	$\log L_{\text{init}}/L_{\odot}$	$M_{\text{WD,ig}}$	$M_{\text{r,ig}}$
N0.7	0.7	-2.118	0.999	0.793
N0.8	0.8	-2.128	1.010	0.862
N0.9	0.9	-2.188	1.039	0.939
N1.0	1.0	-2.137	1.087	1.024
N1.1	1.1	-2.170	1.150	1.114
N1.2	1.2	-2.119	1.225	1.207
R0.8	0.8	-2.114	1.297	1.038
R0.9	0.9	-2.119	1.249	1.050
R1.0	1.0	-2.082	1.207	1.069
R1.1	1.1	-2.050	1.205	1.127

angular momentum of each mass shell decreases over a time step Δt by an amount

$$\Delta j_i = j_i [1 - \exp(-\Delta t/\tau_J)] . \quad (4)$$

Mass accretion from the Keplerian disc is also considered in some model sequences, with different values for the accretion rate (\dot{M}_{acc}). The angular-momentum accretion is treated in the same way as in YL04: the accreted matter is assumed to carry angular momentum at a value close to the Keplerian value if the surface velocity of the central remnant is below critical, while no angular-momentum accretion is allowed otherwise.

Model sequences with different sets of M_{CR} , M_{core} , M_{p} , τ_J , \dot{M} , and T_{p} are calculated, as summarized in Table 2. The initial model in Seqs S is intended to reproduce the result of our SPH simulation, where $M_{\text{CR}} = 1.10 M_{\odot}$ and $M_{\text{p}} \approx 0.84 M_{\odot}$ are adopted. We also assume $M_{\text{CR}} = 1.25 M_{\odot}$ and $M_{\text{p}} \approx 0.9 M_{\odot}$ in Seq. A, and $M_{\text{CR}} = 1.364 M_{\odot}$ and $M_{\text{p}} = 0.95 M_{\odot}$ in Seq. B, to simulate mergers of $0.9 - 1.0 M_{\odot} + 0.7 - 1.0 M_{\odot}$ white dwarf binaries. At a given M_{CR} , different sets of M_{core} , M_{p} , and T_{p} are marked in the sequence label by minor characters (a, b, c, d, e), while different sets of τ_J and \dot{M}_{acc} are indicated by Arabian numbers. For instance, sequences Sa1 – Sa11 have the same initial merger model, but different values for τ_J and \dot{M}_{acc} . Rotation is neglected in a test sequence Ta1 (i.e., the models are non-rotating). The temperature and angular-velocity profiles in the initial central remnant model of Seqs Sa1 – Sa11 are shown in Fig. 6. The temperature (a few to several 10^8 K) and the size ($\sim 10^9$ cm) of the envelope appear to be comparable to those obtained from the SPH simulation (see Fig. 5).

For comparison, we also ran model sequences for classical cold-matter accretion with a constant accretion rate of $\dot{M} = 10^{-5} M_{\odot}/\text{yr}$, for both non-rotating and rotating cases, as summarized in Table 3.

3.2 Results

3.2.1 Classical models of cold-matter accretion

Before discussing the central remnant models, let us first investigate the evolution of classical cold-matter accreting white dwarf models in detail. In these models, the accreted matter is assumed to have the same entropy as the surface value of the accreting white dwarf. As shown in previous studies (e.g. Nomoto & Iben 1985), the thermal evolution of rapidly accreting white dwarfs is deter-

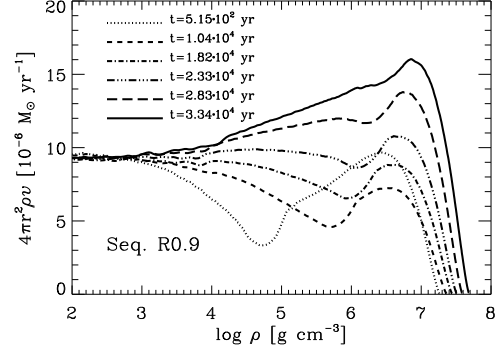


Figure 8. Local effective mass accretion rate ($\dot{M}_{\text{eff,r}} \equiv 4\pi r^2 \rho v$) as a function of density in the models of sequence R0.9, at different evolutionary epochs.

mined by the interplay of compressional heating and thermal diffusion. Fig. 7 shows an example of the evolution of such accreting white dwarf models for an initial WD mass of $0.9 M_{\odot}$ and a constant accretion rate of $\dot{M}_{\text{acc}} = 10^{-5} M_{\odot} \text{ yr}^{-1}$ (Seq. N0.9; Table 3).

Fig. 7a shows that the temperature increases continuously in the envelope ($\rho \lesssim 10^6 \text{ g cm}^{-3}$), and finally carbon burning becomes significant at $\rho \simeq 5.6 \times 10^5 \text{ g cm}^{-3}$ and $T \simeq 6 \times 10^8 \text{ K}$ when $t \simeq 1.3 \times 10^4 \text{ yr}$. In Figs. 7c–f, the rates of compressional heating (ϵ_{comp}), neutrino cooling (ϵ_{ν}), nuclear energy generation (ϵ_{nuc}) and thermal diffusion (ϵ_{th}) are shown. In our stellar evolution code, the compressional heating rate is calculated according to

$$\epsilon_{\text{comp}} = \frac{P}{\rho^2} \left(\frac{\partial \rho}{\partial t} \right)_{M_r} \quad (5)$$

(Kippenhahn & Weigert 1990). Neutrino cooling rates are obtained following Itoh et al. (1996). While ϵ_{comp} , ϵ_{ν} , and ϵ_{nuc} in the figures correspond to the values that are used for the evolutionary calculations, the thermal diffusion rate (ϵ_{th}) – which is only calculated implicitly in the code – can only be estimated to within an order-of-magnitude from

$$\epsilon_{\text{th}} \approx TC_{\text{P}}/\tau_{\text{th}} . \quad (6)$$

Here C_{P} denotes the specific heat at constant pressure, and τ_{th} the local thermal diffusion time scale defined as

$$\tau_{\text{th}} \equiv H_{\text{P}}^2/K , \quad (7)$$

where H_{P} is the pressure scale height, and $K [(4acT^3)/(3C_{\text{PK}}\rho^2)]$ is the thermal diffusivity. It is clear from Fig. 7 that the local peak of temperature is located where the compressional heating rate begins to dominate over the thermal diffusion rate ($\rho \approx 10^5 \text{ g cm}^{-3}$), as expected. The neutrino cooling rate also increases as the temperature in the envelope becomes higher, but nuclear energy generation becomes significant before neutrino cooling dominates the thermal evolution, inducing a carbon-burning flash around $\rho \simeq 5.6 \cdot 10^5 \text{ g cm}^{-3}$.

As Table 3 shows, and consistent with the findings of Nomoto & Iben (1985), such off-center carbon flashes occur regardless of the initial mass of the white dwarf, if $\dot{M}_{\text{acc}} \approx 10^{-5} M_{\odot} \text{ yr}^{-1}$. The results with models including rotation show that carbon ignition may be delayed if the effect of rotation is included (Table 3; see also Piersanti et al. 2003a and Saio & Nomoto 2004). The reason is that the local effective mass accretion rate

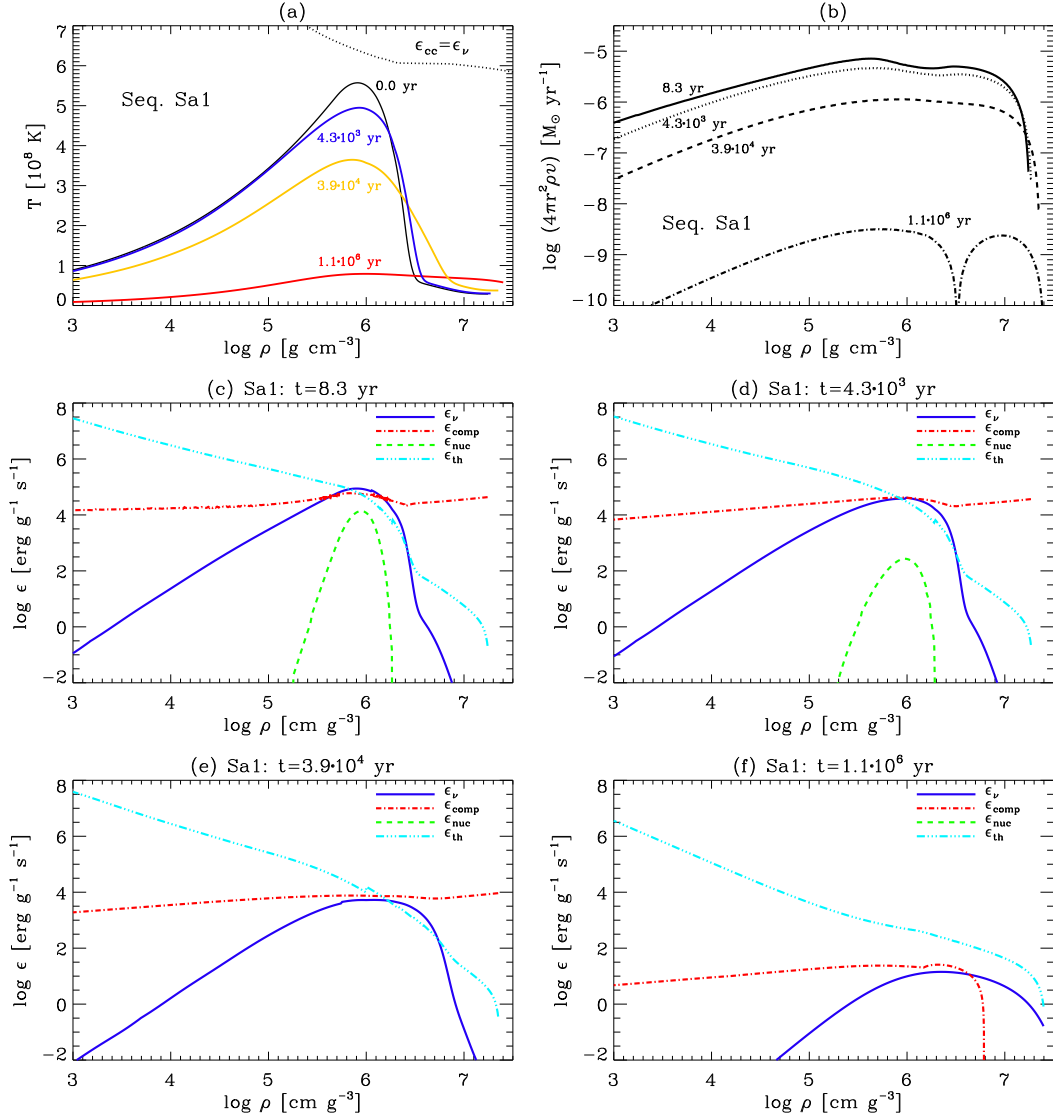


Figure 9. (a) Evolution of the central remnant in Seq. Sa1 in the $\log \rho - T$ plane. The dotted curve gives the critical temperature where the nuclear energy generation rate due to carbon burning equals the energy loss rate due to neutrino cooling. (b) The local effective accretion rate ($\dot{M}_{\text{eff},r} \equiv 4\pi r^2 \rho v_r$) as a function of density in the merger remnant model of Seq. Sa1, at different evolutionary epochs as indicated by the labels. (c) – (f) The rates of energy loss/gain due to neutrino (ϵ_ν) cooling, compressional heating (ϵ_{comp}), nuclear energy generation (ϵ_{comp}) and thermal diffusion (ϵ_{th}) as a function of density in the central remnant models of Seq. Sa1 at different evolutionary epochs. Note that here ϵ_ν , ϵ_{comp} and ϵ_{nuc} represent the values which are used in the evolutionary calculations, while ϵ_{th} is an order-of-magnitude estimate according to Eq. (7).

($\dot{M}_{\text{eff},r} \equiv 4\pi r^2 \rho v$) inside the white dwarf at a given mass is lower because of the centrifugal force. For instance, in Seq. N0.9, we have $\dot{M}_{\text{eff},r} \approx 10^{-5} \text{ M}_\odot \text{yr}^{-1}$ at around $\rho = 5 \times 10^5 \text{ g cm}^{-3}$ when $t \simeq 10^4$ yr (Fig. 7b), but $\dot{M}_{\text{eff},r}$ is lowered by a factor of two in the corresponding rotating model at a similar epoch (i.e., $\dot{M}_{\text{eff},r} \approx 5 \times 10^{-6} \text{ M}_\odot \text{yr}^{-1}$), as revealed in Fig. 8. However, carbon ignition occurs well before the white dwarf reaches the Chandrasekhar limit, in all model sequences considered. Thus, rotation by itself cannot change the conclusion of the previous work that the coalescence of double CO white dwarfs should lead to accretion-induced collapse rather than a thermonuclear explosion, unless the accretion rate is significantly lowered, as was also shown by Piersanti et al. (2003a) and Saio & Nomoto (2004).

3.2.2 Sequences without angular-momentum loss and mass accretion

Having understood the physics of the thermal evolution of CO white dwarfs which accrete cold matter with a rate close to the Eddington limit, we now investigate the evolution of the central remnant model consisting of a cold core and a hot envelope as described in Sect. 3.1. First, we examine the results of the model sequences where both angular-momentum loss and mass accretion from the Keplerian disc are neglected (i.e., $\tau_J = \infty$ and $\dot{M} = 0$; Seqs Sa1, Aa1, Ab1, Ac1, Ad1, Ae1, Ba1, & Ta1).

Fig. 9a illustrates the evolution of the central remnant for $M_{\text{CR}} = 1.10 \text{ M}_\odot$ in Seq. Sa1 in the density – temperature plane. Note that the local peak of temperature at $t = 0.0$ ($T_p = 5.6 \times 10^8 \text{ K}$) is significantly below the critical temperature for car-

bon ignition (T_{C-ig} ; dotted curve in Fig 9a). It is shown in Fig. 9b that the local effective accretion rate ($\dot{M}_{eff,r}$) remains relatively high ($5 \times 10^{-6} - 10^{-5} M_{\odot} \text{ yr}^{-1}$) around $\rho = 10^6 \text{ g cm}^{-3}$, where the local peak of temperature is located, for about 5000 yrs. Despite such high effective accretion rates, the temperature peak continuously decreases, although the inner core becomes somewhat hotter due to compression, and the central remnant finally becomes a cold white dwarf. A few remarkable differences compared to the standard accreting white dwarf models are found in this regard. Firstly, since the envelope is very hot, neutrino cooling – in particular by photoneutrinos – is significant from the beginning, and even dominant over the thermal diffusion at the interface between the core and the envelope as shown in Fig. 9c. In cold-matter accreting white dwarfs, neutrino cooling becomes important only after a significant amount of mass has been accreted (Fig. 7). Secondly, the compressional heating rate is slightly lower than the neutrino cooling rate around the local peak of temperature. As the contraction of the central remnant is mainly determined by the thermal evolution of the envelope, the local accretion rate is in fact controlled by the cooling process. This explains why we have $\epsilon_{comp} \approx \epsilon_{\nu}$ around the local peak of temperature for the initial $\sim 10^4$ yrs, and why the local peak of temperature continuously decreases despite the relatively high effective accretion rate. This conclusion is the same for all other sequences with a T_p that is significantly lower than T_{C-ig} (Seq. Aa1, Ab1, & Ba1) including the non-rotating case (Seq. Ta1; Table 2).

We find that, in Seq. Sa1, the differentially rotating layers at the interface between the core and the envelope in the initial central remnant model are stable against the dynamical shear instability (DSI). They are, however, unstable to the DSI in other sequences, where the interface is more degenerate (see YL04 for discussions on the DSI). Consequently, in Seq. Aa1 for example, the rate of rotational energy dissipation (ϵ_{rot}) appears to be very high initially (Fig. 10). The differentially rotating layers are rapidly smeared out by the dynamical shear instability (see the discussion in Sect. 2 in YL04), and ϵ_{rot} falls below the thermal diffusion and/or neutrino cooling rate only within 20 yrs. Hence we conclude that the rotational energy dissipation does not play an important role for the long-term evolution of the central remnant.

Fig. 11 shows how the evolution of the central remnant changes if the local peak of temperature in the initial model (T_p) is close to or above the critical limit for carbon burning (T_{C-ig}), with Seqs Ac1 and Ae1 as examples. In contrast to Seq. Sa1 or Aa1, carbon burning dominates the evolution very soon in both sequences, and the temperature increases rapidly. Although the further evolution has not been followed in the present study, it is most likely that the carbon-burning flame propagates inward such that the central remnant is converted into an ONeMg white dwarf within several thousand years as shown by Saio & Nomoto (1998).

As summarized in Table 2, all other sequences follow the same evolutionary pattern: off-center carbon ignition is avoided in Seqs Ab1, Ba1, and Ta1 where T_p is significantly below T_{C-ig} , while carbon ignites off-center in the other sequences where $T_p \gtrsim T_{C-ig}$. It is thus remarkable that the thermal evolution of the central remnant is sensitively determined by the local peak of temperature in the quasi-static equilibrium state.

In conclusion, in the absence of angular-momentum loss and mass accretion from the Keplerian disc, the thermal evolution of the central remnant is roughly controlled by neutrino cooling at the interface between the core and the envelope, and off-center carbon burning may be avoided as long as $T_p < T_{C-ig}$, while it seems inevitable if $T_p \gtrsim T_{C-ig}$.

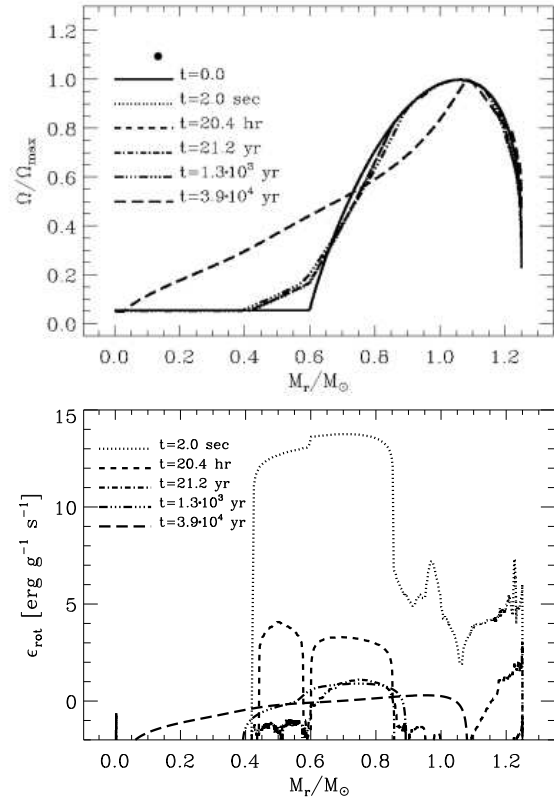


Figure 10. Upper panel: The angular velocity relative to the local maximum as a function of the mass coordinate in the central remnant models of Seq. Aa1 at different evolutionary epochs. Lower panel: the rate of rotational energy dissipation (ϵ_{rot} ; see YL04) as a function of the mass coordinate in the corresponding models shown in the upper panel.

3.3 Effect of angular momentum loss

In Seqs Sa2 – Sa5, the central remnant has the same initial conditions as in Seq. Sa1, angular momentum loss from the white dwarf with different time scales τ_J is considered according to Eq. (4). Note that off-center carbon ignition occurs in Seqs Sa2, Sa3 & Sa4, where $\tau_J \lesssim 10^4$ yr, while it is avoided in Seq. Sa5 where $\tau_J = 10^5$ yr. These results indicate that off-center carbon ignition should be induced if the angular-momentum loss occurs too rapidly for neutrino cooling or thermal diffusion to control the effective mass accretion. For instance, Fig. 12 shows that in Seq. Sa4, where $\tau_J = 10^4$ yr, the effective mass accretion rate reaches a few $10^{-5} M_{\odot} \text{ yr}^{-1}$ at the interface between the core and the envelope ($\rho \approx 10^6 \text{ g cm}^{-3}$), and the compressional heating rate exceeds the neutrino cooling rate.

It is shown that the critical angular-momentum-loss time scale, τ_J , for off-center carbon ignition ($\tau_{J,crit}$) is smaller for Seqs Ab and Ba than for Seqs Sa and Aa: $\tau_{J,crit} \approx 10^3$ for Seqs Ab and Ba, and $\tau_{J,crit} \approx 10^4$ for Seqs Sa and Aa. This is due to the different local thermodynamic properties at the interface between the core and the envelope in different central remnant models. As shown in Fig. 13, higher density and/or temperature at the interface result in a shorter neutrino cooling time, making it possible to avoid local heating for a smaller τ_J . In other words, $\tau_{J,crit}$ roughly corresponds to the time scale for neutrino cooling at the local peak of temperature ($\tau_{\nu,p}$).

From this experiment, we conclude that, in the absence of

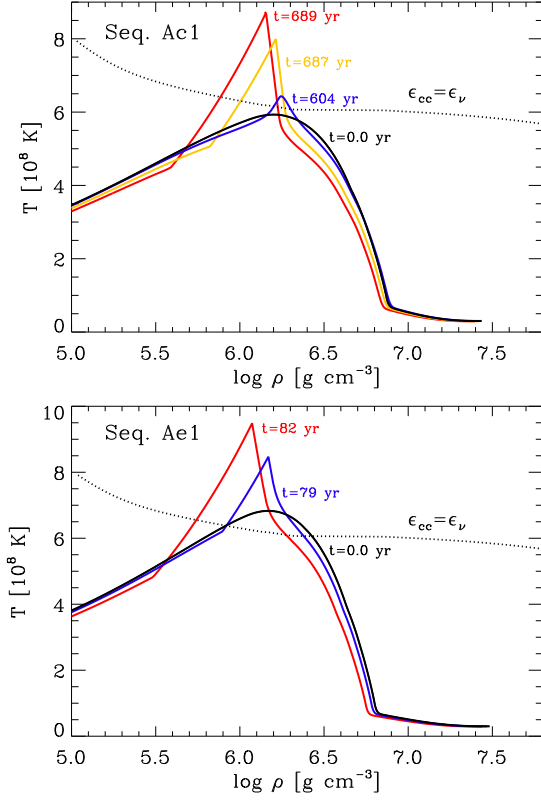


Figure 11. Evolution of the central remnant in Seqs Ac1 (upper panel) and Ae1 (lower panel), in the $\log \rho - T$ plane. The dotted curve gives the critical temperature where nuclear energy generation rate due to carbon burning equals to energy loss rate due to neutrino cooling.

mass accretion from the Keplerian disc, carbon ignition may be avoided in the central remnant, if $T_{\max, \text{init}} < T_{C-\text{ig}}$, and if $\tau_J > \tau_{\nu, p}$.

3.4 Mass accretion from the Keplerian disc

In reality, mass accretion from the Keplerian disc onto the central remnant is expected. The accretion rate is determined by the viscosity of the disc, which is not well known. However, we expect the accretion rate from a Keplerian disc may be significantly lower than from a pressure-supported thick disc that was assumed in previous studies. Our results, as summarized in Table 2, indicate that even with mass accretion, the central remnant with $T_p < T_{C-\text{ig}}$ can avoid off-center carbon ignition if the accretion rate is sufficiently low (i.e., $\dot{M} < 5 \times 10^{-6} \dots 10^{-5} M_\odot \text{ yr}^{-1}$), and if $\tau_J > \tau_{\nu, p}$ (see Table 2).

The thermal history of the central remnant in those sequences where carbon ignites off-center is similar to that of the white dwarf in classical accretion model sequences. However, as the central remnant has a rapidly rotating hot envelope, carbon ignition is significantly delayed compared to the case of classical accretion. In Seq. N1.2, where $M_{\text{init}} = 1.2 M_\odot$ and $\dot{M}_{\text{acc}} = 10^{-5} M_\odot \text{ yr}^{-1}$, carbon ignites only when about $0.025 M_\odot$ is accreted, while in Seq. Aa7 more than $0.15 M_\odot$ have to be accreted to induce carbon ignition at the same accretion rate, despite its higher initial mass. On the other hand, the comparison of Seq. Aa7 with Seq. Aa10 indicates that off-center carbon ignition is delayed if the central remnant keeps more angular momentum. The critical accretion rate

for inducing off-center carbon ignition is thus difficult to precisely determine, as our 1-D models significantly underestimate the effect of the centrifugal force, especially in the envelope where carbon ignites. In addition, the physics of angular momentum loss/gain is not well understood yet, as discussed in Yoon & Langer (2005).

Note that $M_{\text{WD,ig}}$ in Seqs Aa10, Ba6 and Ba7 is already very close, or even above the Chandrasekhar limit. However, the central density in those models is still smaller by an order of magnitude than the critical limit for carbon ignition due to the effect of rotation. As the carbon-burning flame will propagate inwards within several thousand years (Saio & Nomoto 1998), only about $\sim 0.05 M_\odot$ may be further accreted by the time the burning flame reaches the center, and the central density may not become high enough to induce a thermonuclear explosion before the whole central remnant is converted into an ONeMg white dwarf. (Super-) Chandrasekhar mass ONeMg white dwarfs produced in this way will eventually collapse to a neutron star (see Yoon & Langer 2005; Dessart et al. 2006).

On the other hand, the white dwarf continuously grows to/above the Chandrasekhar limit ($\approx 1.4 M_\odot$) without suffering carbon ignition (neither at the center nor off-center) in Seqs Sa8, Sa9, Sa10, Sa11, Aa8, Aa9, Ab6, and Ba8. The outcome in these cases is thus the formation of a (super-) Chandrasekhar mass CO white dwarf, which will eventually explode as a Type Ia supernova. The mass of the exploding white dwarf should depend on the amount of angular momentum (Yoon & Langer 2005) and cannot exceed the mass budget of merging white dwarfs. Fig. 14 shows the evolutionary paths of the central remnant for Seqs Sa8, Sa9 & Sa11 as examples in the mass – angular momentum plane. Note that the central remnant initially has a large amount of angular momentum ($J = 1.11 \times 10^{50} \text{ erg s}$), such that without loss/gain of angular momentum, it should accrete matter until it reaches $M \simeq 1.68 M_\odot$ where it explodes in a SN Ia explosion. In Seqs Sa8 and Sa9, the accretion time scale (τ_{acc}) is longer than the angular momentum loss time scale, and the total angular momentum of the white dwarf continuously decreases while the total mass increases. Consequently, carbon ignites at the center when the white dwarf grows to $1.50 M_\odot$ and $1.42 M_\odot$ for Seqs Sa8 and Sa9, respectively. In Seq. Sa11, on the other hand, both mass and angular momentum of the central remnant continuously increase, given that $\tau_{\text{acc}} \lesssim \tau_J$, and a SN Ia explosion is expected only when $M \simeq 1.70 M_\odot$. Note that this is even larger than the mass budget of the binary system considered for this sequence (i.e., $0.9 M_\odot + 0.6 M_\odot$). In nature, the white dwarf must stop growing in mass when $M = 1.5 M_\odot$, and a SN Ia explosion will be induced only when a sufficient amount of angular momentum has been removed, e.g. via gravitational wave radiation, as illustrated by the path Sa11-B in Fig. 14.

4 CONCLUSION AND DISCUSSION

We have explored the dynamical and secular evolution of the merger of double CO white dwarf binaries whose total mass exceeds the Chandrasekhar limit. Based on our new SPH simulation of the coalescence of two CO white dwarfs of $0.9 M_\odot$ and $0.6 M_\odot$, we suggest that the immediate post-merger remnant is best described as a differentially rotating CO star consisting of a slowly rotating cold core and a rapidly rotating hot envelope that is surrounded by a Keplerian disc rather than as “cold white dwarf + thick disc” system, as in previous investigations. The evolution of such a CO star is determined by the thermal evolution of the envelope, and the growth of the core is controlled by the cooling due

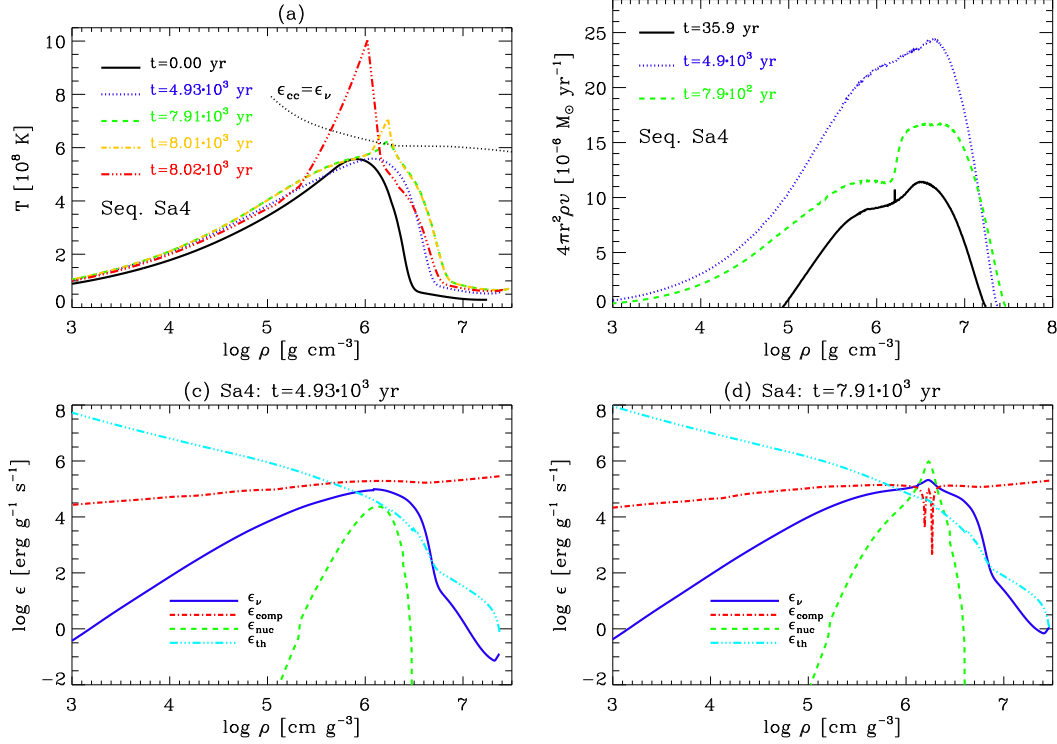


Figure 12. Same as in Fig. 9, but for Seq. Sa4.

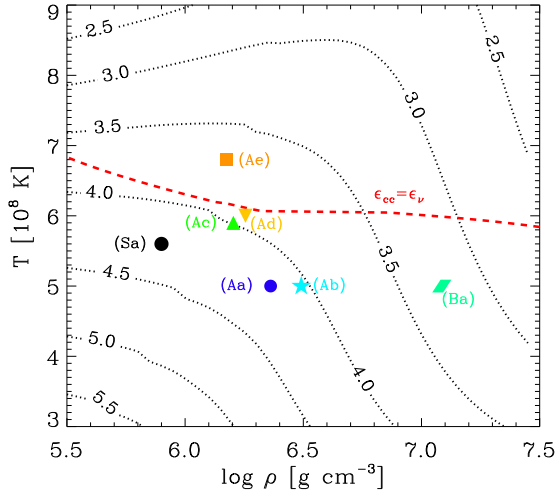


Figure 13. Contour lines of the neutrino cooling time scale ($\tau_\nu \equiv TC_p/\epsilon_\nu$) in the $\log \rho - T$ plane. The level at each line gives $\log \tau_\nu$ in units of years. The dashed line denotes the critical temperature for carbon ignition. The local peak of temperature and the corresponding density in the initial model of Seqs Sa, Aa, Ab, Ac, Ae, and Ba are marked by the filled symbols as indicated by the labels.

to neutrino emission and thermal diffusion, which is fundamentally different from the assumption of “forced accretion of cold matter”.

Our 1-D stellar evolution models of the central remnant, i.e. the cold core and the hot envelope, which include the effects of rotation, indicate that there are three necessary conditions for the

merger remnant to avoid off-center carbon ignition such that a SN Ia may be produced:

- (i) The local peak of temperature of the merger remnant at the interface between the core and the envelope must be lower than the critical temperature for carbon ignition ($T_p < T_{C-ig}$).
- (ii) The time scale for angular-momentum loss from the central remnant by must be larger than the neutrino cooling time scale at the interface ($\tau_J > \tau_{\nu,P}$).
- (iii) Mass accretion from the Keplerian disc onto the central remnant must be sufficiently slow ($\dot{M}_{acc} \lesssim 5 \times 10^{-6} \dots 10^{-5} M_\odot \text{ yr}^{-1}$).

Our new SPH simulation confirms that at least the first condition ($T_p < T_{C-ig}$) should be fulfilled in the CO white dwarf binary considered.

As emphasized in Sect. 3.1, our 1-D models significantly underestimate the effect of the centrifugal force on the stellar structure in the rapidly rotating outermost layers. However, since thermal diffusion always dominates over both neutrino cooling and compressional heating in the outer envelope ($\rho \lesssim 10^5 \dots 10^6 \text{ g cm}^{-3}$) above the interface, as shown in Figs. 7 and 12, the detailed structure of the rapidly rotating outermost layers above the interface may not significantly affect our results on the thermal evolution of the merger remnant, as long as the angular momentum of the envelope is not lost faster than the local neutrino cooling time scale at the interface. On the other hand, mass accretion from the Keplerian disc should occur preferentially along the equatorial plane of the envelope. As shown in the SPH simulation, the envelope is more extended along the equatorial plane, where most angular momentum is deposited, than along the polar axis, and the resultant compressional heating must be much weakened, compared to the case of our 1-D models. The enhanced role of rotation must thus help

to increase the critical mass accretion rate for inducing off-center carbon ignition, in favor of producing a Type Ia supernova.

We have concluded that the loss of angular momentum on a short time scale ($\tau_J \lesssim \tau_{\nu,p} \approx 10^4 \dots 10^5$ yr) may induce off-center carbon ignition even when $T_{\max, \text{init}} < T_{C-\text{ig}}$. Rapidly rotating compact stars may experience loss of angular momentum by gravitational wave radiation, due to either the bar-mode instability or the r-mode instability. The onset of the dynamical or secular bar-mode instability requires a very high ratio of the rotational energy to the gravitational energy: $E_{\text{rot}}/E_{\text{grav}} \gtrsim 0.2$ for the dynamical bar-mode instability, and $E_{\text{rot}}/E_{\text{grav}} \gtrsim 0.14$ for the secular bar-mode instability (e.g. Shapiro & Teukolsky 1983). As both our 1-D models and SPH simulation give a value of $E_{\text{rot}}/E_{\text{grav}}$ that is much lower (about 0.06 – 0.07) than those critical limits, the bar-mode instability may not be relevant. The r-mode instability may operate, in principle, even with such a low $E_{\text{rot}}/E_{\text{grav}}$ (Andersson 1998; Friedman & Morsink 1998). However, we estimate that the growth time of the r-mode instability (τ_r), using our central remnant models and following Lindblom (1999), is $\gtrsim 10^6$ yr, which is much longer than the local neutrino cooling time scale ($\tau_{\nu,p} \approx 10^4$ yr). Alternatively, angular momentum might be transported from the accreting star into the Keplerian disc when the accretor reaches critical rotation. Calculations by Saio & Nomoto (2004) indicate, however, that the decrease of the total angular momentum due to such an effect is not significant in accreting white dwarfs. In conclusion, neither gravitational wave radiation nor outward angular-momentum transport is likely to lead to a rapid loss of angular momentum from the central remnant such that $\tau_J < \tau_{\nu,p}$, unless magnetic torques are important.

The central remnant may be enforced to rotate rigidly on a short time scale in the presence of strong magnetic torques (cf. Spruit 2002). The central remnant in both our SPH simulation and 1-D models has $J_{\text{tot}} > 10^{50}$ erg s, which is significantly higher than the maximum limit a rigidly rotating white dwarf can retain, as shown in Fig. 14. This means that if magnetic torques led to rigid rotation, a large amount of angular momentum should be transported into the Keplerian disc (Case *a* in Fig. 14), or mass shedding of super-critically spun-up layers should occur from the central remnant (Case *b* in Fig. 14). In Case *a*, the local density around the interface should increase by several factors by the time when the central remnant reaches rigid rotation as implied by Fig. 15. Off-center carbon ignition might be inevitable in this case due to a resultant high effective accretion rate, if the time for angular momentum redistribution were shorter than the local cooling time due to neutrino losses. In Case *b*, on the other hand, the local density at the interface might not increase if mass shedding from the central remnant occurred at a sufficiently high rate. Therefore, the role of magnetic fields in the merger evolution remains uncertain at the current stage and is a challenging subject for future work.

The coalescence of more massive double CO white dwarf binaries is likely to result in a higher maximum temperature due to the enhanced role of gravity. Consequently, given the important role of the maximum temperature in the merger remnant for its final fate, less massive binary CO white dwarfs may be favored for the production of SNe Ia from such a channel.

We note that there are number of potentially important factors that have not been included in either the present study or previous simulations. These include the following points:

(i) The previous and present simulations assumed that white dwarfs are cold prior to the merging process. However, Iben, Tutukov & Fedorova (1998) point out that tidal interactions

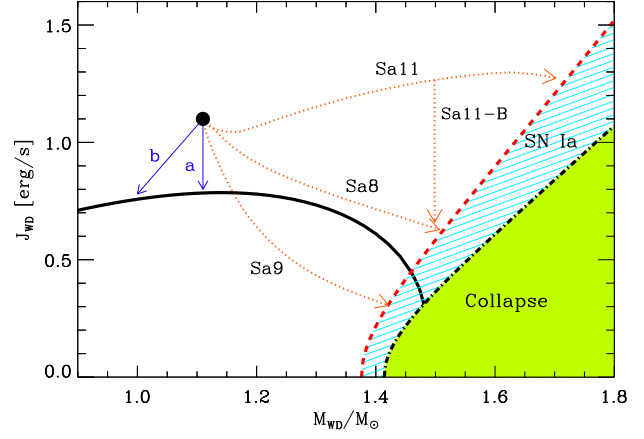


Figure 14. Evolution of the central remnant in the mass – angular momentum plane. The thick solid curve shows the angular momentum of a rigidly rotating white dwarf with critical rotation at the surface as a function of the white dwarf mass. The thick dashed curve and the thick dot-dashed curve give the critical angular momentum for a differentially rotating CO white dwarf to reach carbon ignition at the center ($\rho_c = 2 \times 10^9$ g cm $^{-3}$), and electron-capture induced collapse ($\rho_c = 10 \times 10^{10}$ g cm $^{-3}$), respectively, according to Yoon & Langer (2005). A SN Ia explosion is expected in the hatched region. The filled circle denotes the initial model of the central remnant in Seq. Sa. The evolution of the central remnant in Seqs Sa 8, Sa9 and Sa11 is shown by the thin dotted curves, as indicated. The thin solid curves denote possible evolutionary paths of the central remnant with strong magnetic torques that may enforce rigid rotation, with loss of angular momentum but without mass shedding (Case ‘a’), and with both loss of angular momentum and mass shedding (Case ‘b’). See the text for more details.

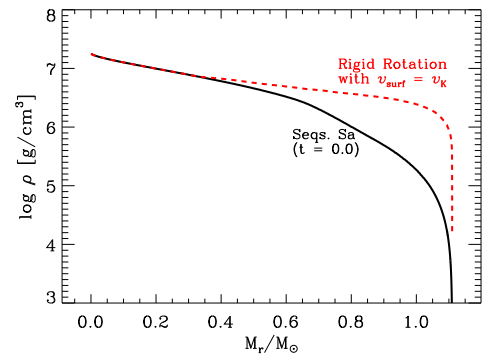


Figure 15. The density profile in the initial model of the central remnant in Seqs Sa (solid curve), and in a corresponding hot ($T_c = 10^8$ K) white dwarf model that rotates rigidly at critical rotation at the surface (dashed curve).

might heat up the white dwarfs as the orbit shrinks, which could weaken the gravitational potential of the primary. Furthermore, as the temperature of white dwarfs is a function of their age, younger progenitors should have more extended envelopes, which may result in a lower T_p .

(ii) A thin hydrogen/helium envelope must be present initially in both the primary and the secondary. As hydrogen or helium should ignite at a much lower temperature than carbon, the influence of the release of nuclear energy during the merger process may be even more important than shown in the existing SPH simulations,

which is likely to lower T_p . Furthermore, neutrino losses, which were neglected in the present study, would also tend to reduce T_p .

(iii) At a given total mass ($M_{\text{tot}} = M_{\text{primary}} + M_{\text{secondary}}$), different mass ratios of the white dwarf components ($q \equiv M_{\text{secondary}}/M_{\text{primary}}$) must result in different merger structures.

(iv) A lower q at a given M_{tot} may not only lead to a stronger gravitational potential of the primary, but also to a lower mass accretion rate during the dynamical mass transfer (Guerrero et al. 2004). As the former and the latter will tend to increase and decrease T_p , respectively, quantitative studies are necessary to predict how T_p will change with q .

Finally, another important ingredient that needs to be considered is thermal diffusion during the dynamical evolution. As shown above, the mass-accretion rate from the Keplerian disc onto the envelope of the central remnant is one of the most important factors that critically determine the final fate of double CO white dwarf mergers. The accretion rates depend on the structure of the Keplerian disc at thermal equilibrium, which can be only understood by including thermal diffusion in future simulations. But here we emphasize again that the accretion rates from a centrifugally supported Keplerian disc should be significantly lower than those from a pressure-supported thick disc that was previously assumed, which opens the possibility for at least some double CO white dwarf mergers to produce SNe Ia.

ACKNOWLEDGMENTS

We are grateful to Norbert Langer and Ken'ichi Nomoto for many useful suggestions and comments. SCY is supported by the VENI grant (639.041.406) of the Netherlands Organization for Scientific Research (NWO). The computations have been performed on the JUMP supercomputer at the Höchstleistungsrechenzentrum Jülich.

REFERENCES

- Andersson, N., 1998, *ApJ*, 502, 708
 Balsara, D.S., 1995, *JCoPh.*, 121, 357
 Benz, W., Cameron, A.G.W., Press, W.H., & Bowers, R.L., 1990, *ApJ*, 348, 647
 Branch, D., Livio, M., Yungelson, L. R., Boffi, F.R., Baron, E., 1995, *PASP*, 107, 1019
 Dessart, L., Burrows, A., Ott, C., Livne, E., Yoon, S.-C., & Langer, N., 2006, *ApJ*, 644, 1063
 Friedman, J.L., & Morsink, S.M., 1998, *ApJ*, 502, 714
 Guerrero, J., García-Berro, E., & Isern, J., 2004, *A&A*, 413, 257
 Hix, W.R. et al., 1998, *ApJ*, 503, 332
 Iben, I. Jr., & Tutukov, A., 1984, *ApJS*, 55, 335
 Iben, I.Jr., Tutukov, A.V., & Fedorova, A.V., 1998, *ApJ*, 503, 344
 Itoh, N., Hayashi, H., Hishikawa, A., & Kohyama, Y., 1996, *ApJS*, 102, 411
 Kippenhahn, R., & Weigert, A., 1990, *Stellar Structure and Evolution*, Springer-Verlag
 Knaap, R.C.J., 2004, Master Thesis, Utrecht University
 Lomax, H., Pulliam, T.H. and Zingg, D.W., 2001, *Fundamentals of Computational Fluid Dynamics*, Springer, Heidelberg
 Lindblom, L., 1999, *Phys. Rev. D*, 60, 4007
 Mochkovitch, R., & Livio, M., 1989, *A&A*, 209, 111
 Mochkovitch, R., & Livio, M., 1990, *A&A*, 236, 378
 Monaghan, J.J., & Varnas, S.R., 1988, *MNRAS*, 231, 515
 Monaghan, J.J., 2002, SPH compressible turbulence, *MNRAS* 335, 843
 Morris, J.P., & Monaghan, J.J., 1997, *J. Comp. Phys.*, 136, 41
 Napiwotzki, R., Karl, C., & Nelemans, G. et al., 2004, *RMxAC*, 20, 113
 Napiwotzki, R., Koester, D., & Nelemans, G., et al., 2002, *A&A*, 386, 957
 Nomoto, K., & Iben, I.Jr., 1985, *ApJ*, 297, 53
 Nomoto, K., & Kondo, Y., 1991, *ApJ*, 367, L19
 Paczyński, B., 1991, *ApJ*, 370, 597
 Piersanti, L., Gagliardi, S., Iben, I.Jr., & Tornambé, A., 2003a, *ApJ*, 583, 885
 Piersanti, L., Gagliardi, S., Iben, I.Jr., & Tornambé, A., 2003b, *ApJ*, 598, 1229
 Popham, R., & Narayan, R., 1991, *ApJ*, 370, 604
 Price, D., 2004, PhD thesis (Cambridge)
 Price, D. & Monaghan, J.J., accepted by *MNRAS*, [astro-ph/0610872]
 Rosswog, S., & Davies, M.B., 2002, *MNRAS*, 334, 481
 Rosswog, S., Davies, M.B., Thielemann, F.-K., & Piran, T., 2000, *A&A*, 360, 171
 Rosswog, S., & Liebendörfer, M., 2003, *MNRAS*, 342, 673
 Rosswog, S., Ramirez-Ruiz, E. and Hix, W.R., to be submitted
 Rosswog, S., Speith, R. & Wynn, G., 2004, *MNRAS*, 351, 1121
 Saio, H., & Nomoto, K., 1985, *A&A*, 150, 21
 Saio, H., & Nomoto, K., 1998, *ApJ*, 500, 388
 Saio, H., & Nomoto, K., 2004, *ApJ*, 615, 444
 Segretain, L., Chabrier, G., & Mochkovitch, R., 1997, *ApJ*, 481, 355
 Shapiro, S.L., & Teukolsky, S.A., 1983, *Black Holes, White Dwarfs and Neutron Stars: The Physics of Compact Objects*, Wiley-Interscience
 Springel, V. & Hernquist, L., 2002, *MNRAS*, 333, 649
 Spruit, H.C., 2002, *A&A*, 381, 923
 Tutukov, A.V., & Yungelson, L., 1979, *Acta. Astr.*, 29, 665
 Timmes, F.X. & Swesty, F.D., 2000, *ApJS*, 126, 501
 Webbink, R.F., 1984, *ApJ*, 277, 355
 Yoon, S.-C., & Langer, N., 2004, *A&A*, 419, 623 (YL04)
 Yoon, S.-C., & Langer, N., 2005, *A&A*, 435, 967

(a) (a)

